Supplementary Information

Ultrathin $CuBi_2O_4$ on bipolar Bi_2O_3 nano-scaffold: self-powered broadband photoelectrochemical photodetector with improved responsivity and response speed

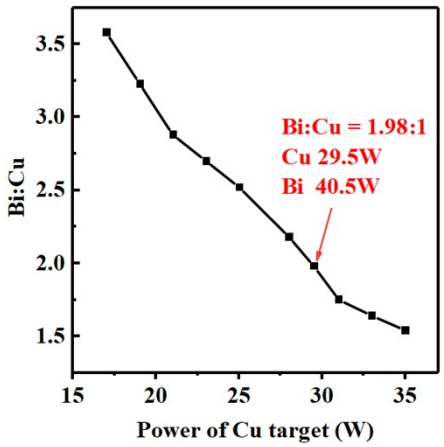

Figure S1. The Bi to Cu ratios of $CuBi_2O_4$ films as a function of the power of Cu target; The power of Bi target remained 40.5W; The ratio of Bi to Cu was detected by the ICP-MS.

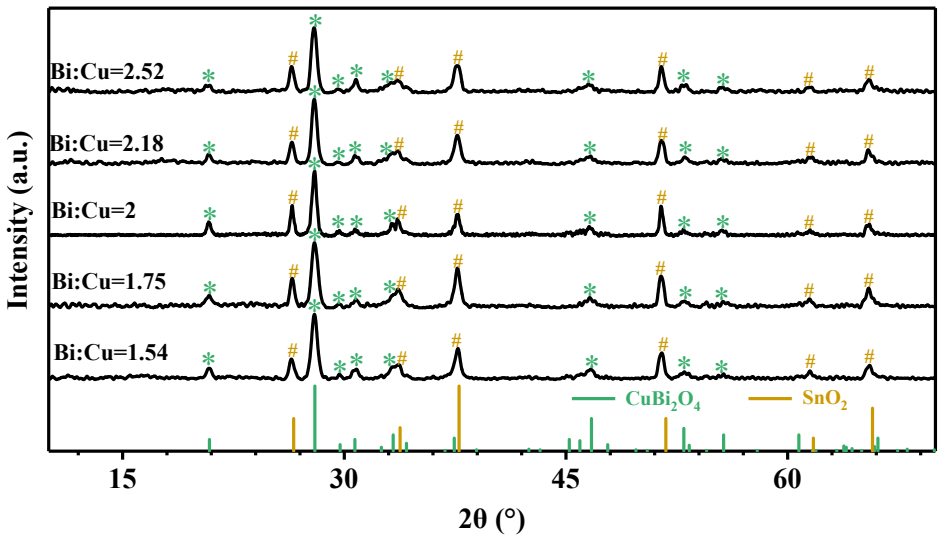

Figure S2. XRD spectra for $CuBi_2O_4$ films on FTO substrates with different Bi to Cu

ratios.

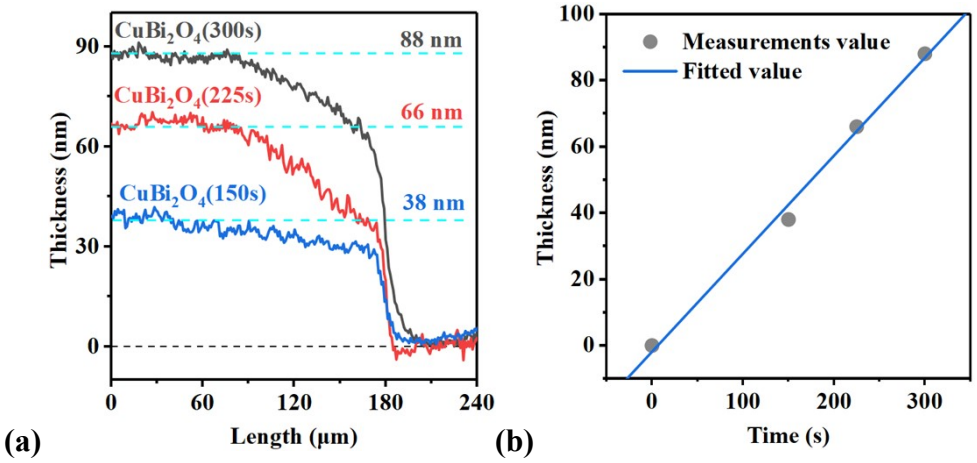

Figure S3. (a) Scanning results of optical profiler for $CuBi_2O_4$ films with different deposition time; (b) Thickness of $CuBi_2O_4$ films with different deposition time, where points and line represented measurement results and fitting results, respectively.

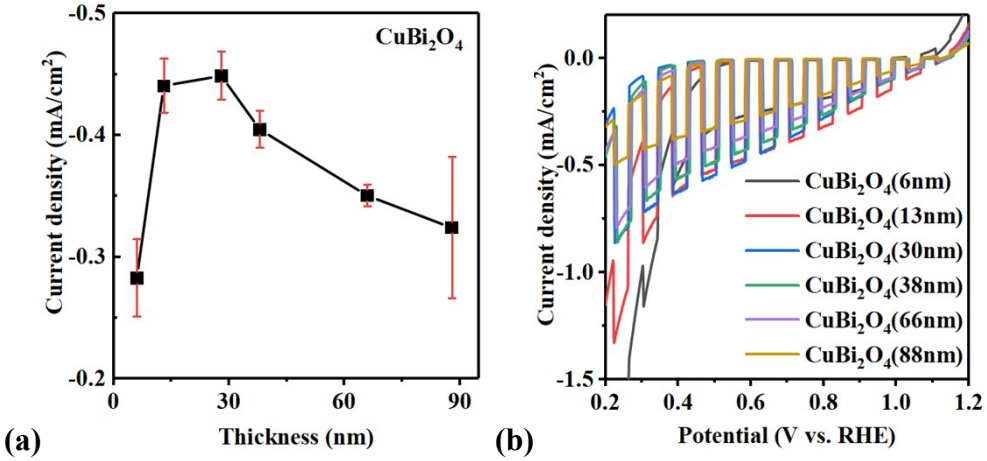

Figure S4. (a) Current density for $CuBi_2O_4$ photoelectrodes with different film thickness; (b) Chopped LSV scans for $CuBi_2O_4$ photoelectrodes with different film thickness. The measurements were performed under AM 1.5 illumination.

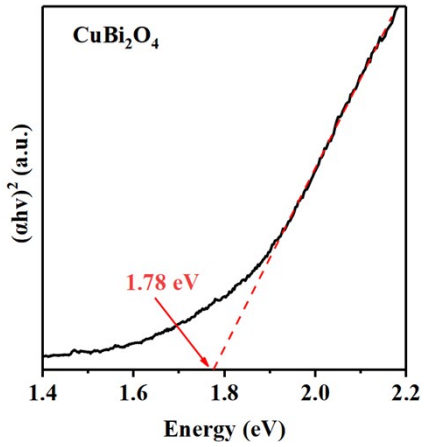

Figure S5. Tauc plots for $CuBi_2O_4$(100s) film.

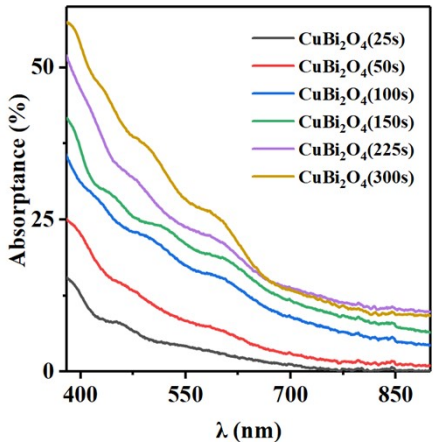

Figure S6. Absorption spectra for $CuBi_2O_4$ films with different thickness.

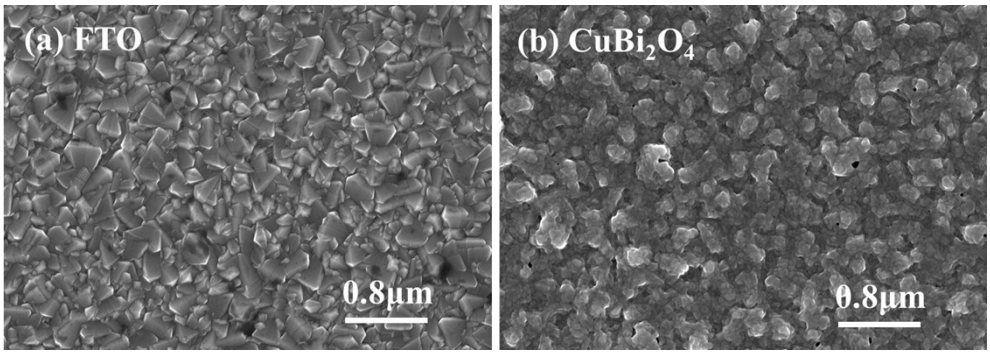

Figure S7. SEM images of (a) pure FTO and (b) ~30 nm $CuBi_2O_4$.

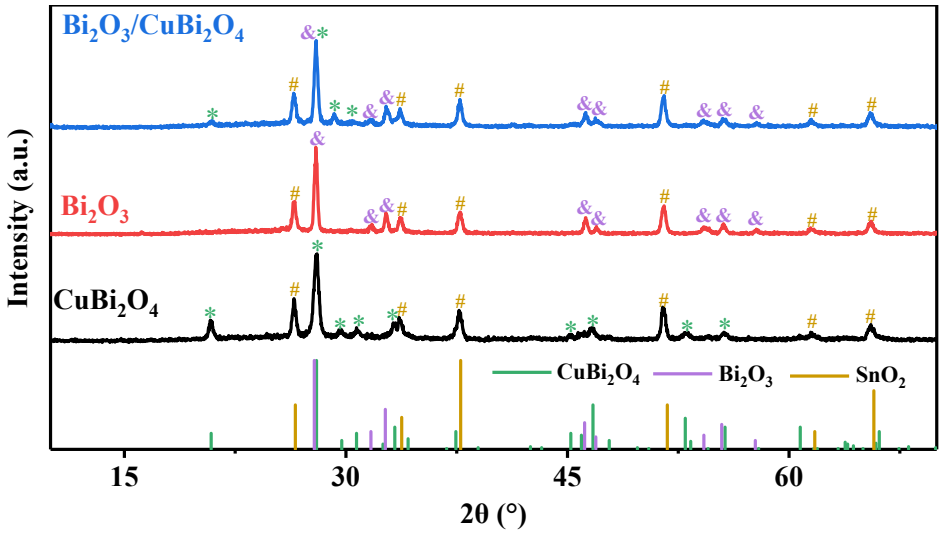

Figure S8. XRD spectra for $CuBi_2O_4$ Bi_2O_3 and $Bi_2O_3/CuBi_2O_4$ films.

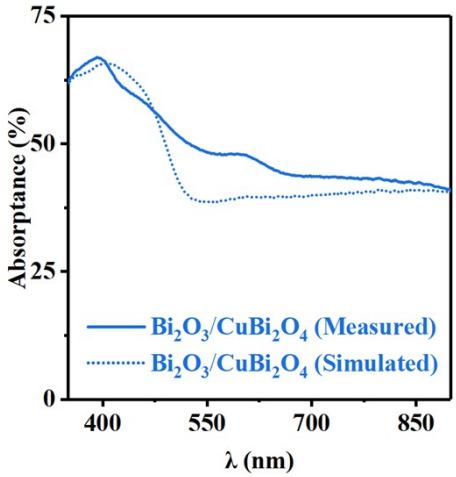

Figure S9. Measured and simulated (Bi_2O_3 + $CuBi_2O_4$) absorption for $Bi_2O_3/CuBi_2O_4$ film.

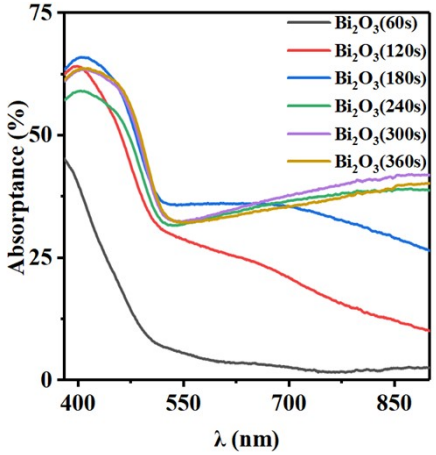

Figure S10. Absorption spectra for Bi_2O_3 films with different deposition time.

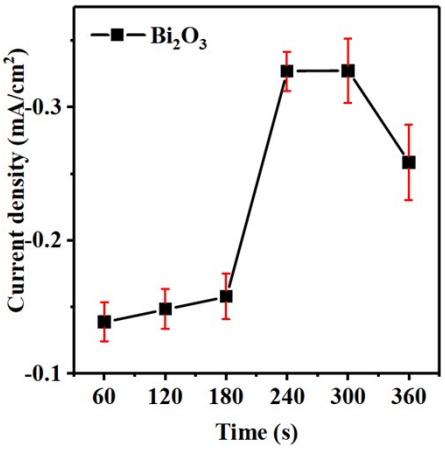

Figure S11. Current density for Bi_2O_3 photoelectrodes with different deposition time. The measurements were performed under AM 1.5 illumination.

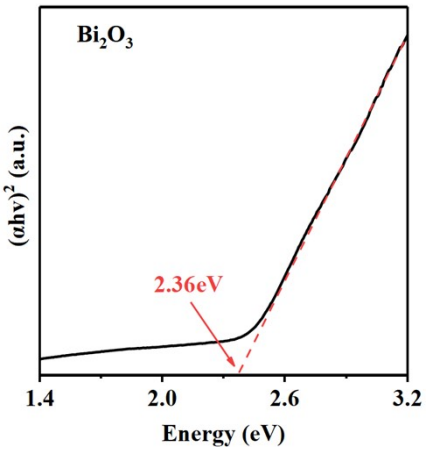

Figure S12. Tauc plots for $CuBi_2O_4$(240s) film.

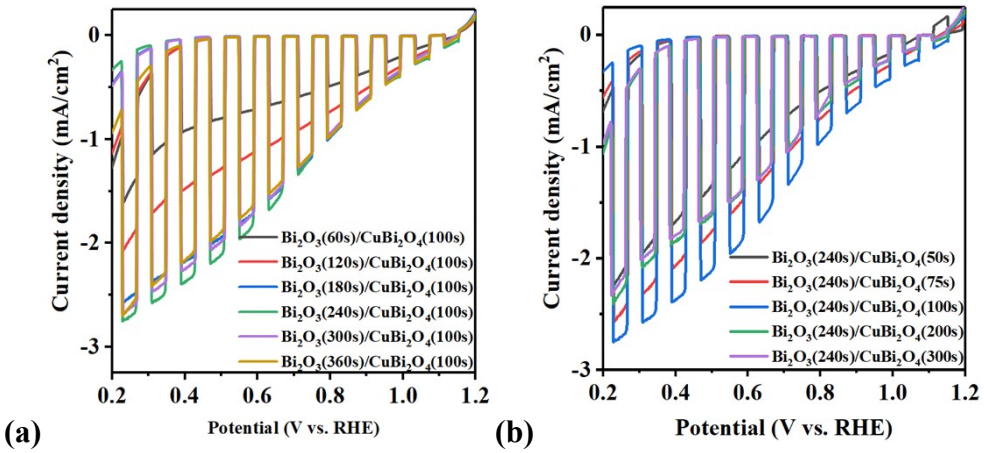

Figure S13. Chopped LSV scans for $Bi_2O_3/CuBi_2O_4$ photoelectrodes; (a) The deposition time of $CuBi_2O_4$ remains unchanged for 100s, and the deposition times of Bi_2O_3 were changed between 60s-360s; (b) The deposition time of Bi_2O_3 remained

unchanged for 240s, and the deposition times of $CuBi_2O_4$ were changed between 50s-300s. The measurements were performed under AM 1.5 illumination.

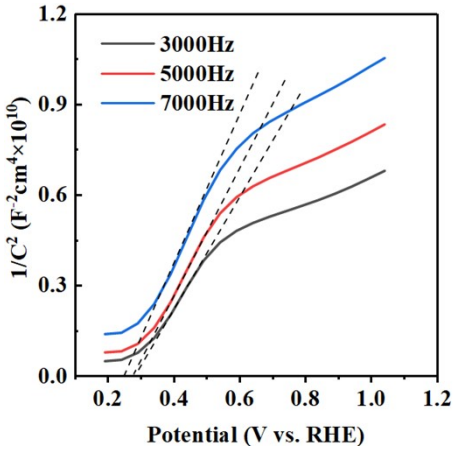

Figure S14. Mott–Schottky plots for FTO.

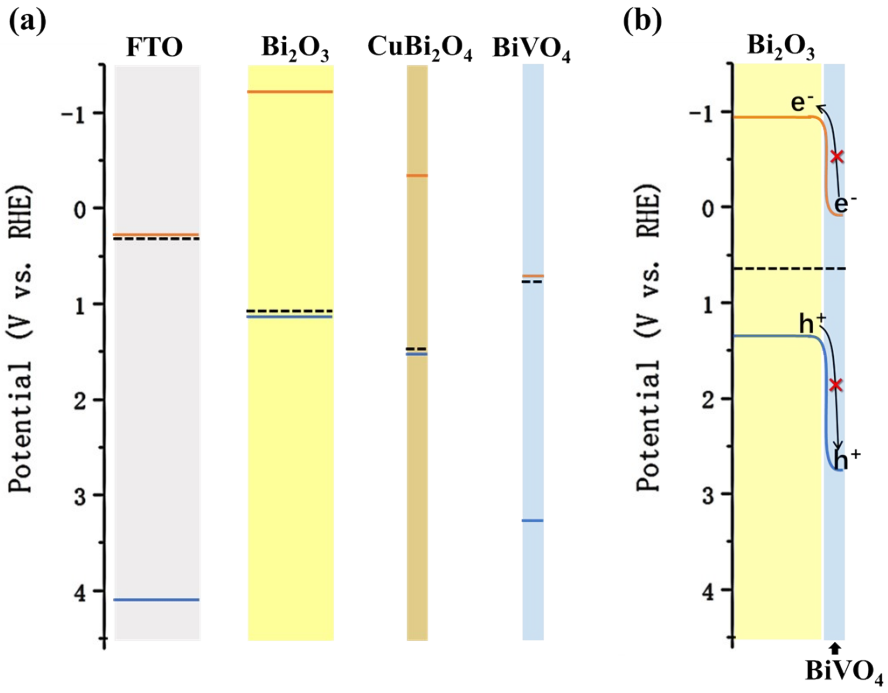

Figure S15. (a) Estimated band diagrams of FTO, Bi_2O_3, $CuBi_2O_4$ and $BiVO_4$; (b) Estimated band diagrams of $Bi2O_3/BiVO_4$, where the orange solid line, the blue solid line and the black dashed line represented the CB, VB, and Fermi energy level, respectively.

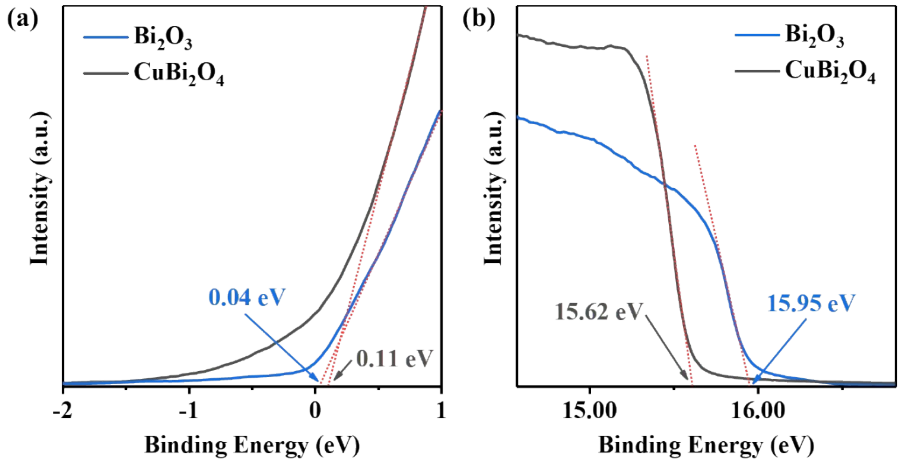

Figure S16: UPS of Bi_2O_3 and $CuBi_2O_4$ tested at (a) 0 V bias and (b) -5 V bias, respectively.

As shown in Figure S16a, the Fermi level of Bi_2O_3 and $CuBi_2O_4$ lied 0.04 eV and 0.11 eV above the VB edge, respectively. As shown in Figure S16b, the work function of Bi_2O_3 and $CuBi_2O_4$ were estimated to be 5.27 eV (21.22 eV – 15.95 eV = 5.27 eV) and 5.60 eV (21.22 eV – 15.62 eV = 5.60 eV), respectively.

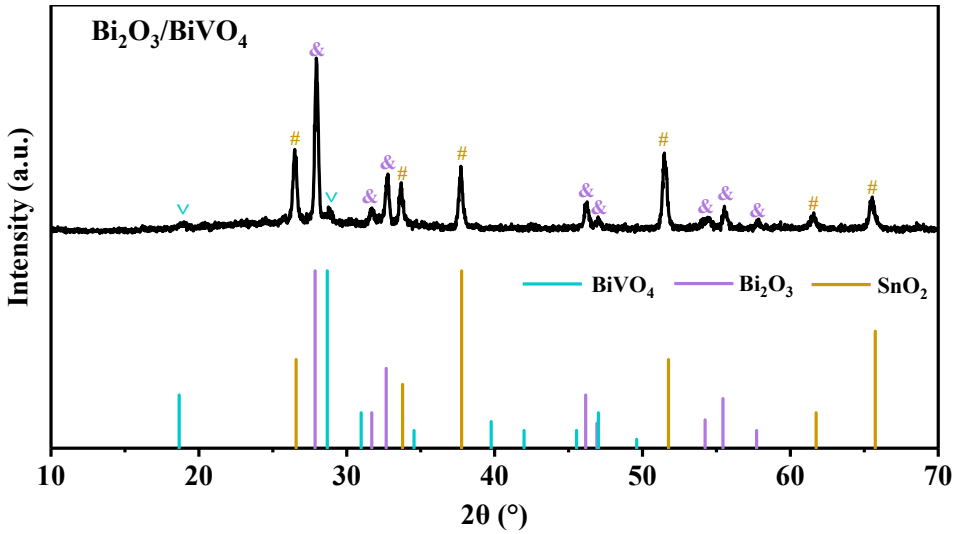

Figure S17. XRD spectra for $Bi2O_3/BiVO_4$ film on FTO substrate, blue represents $BiVO_4$.

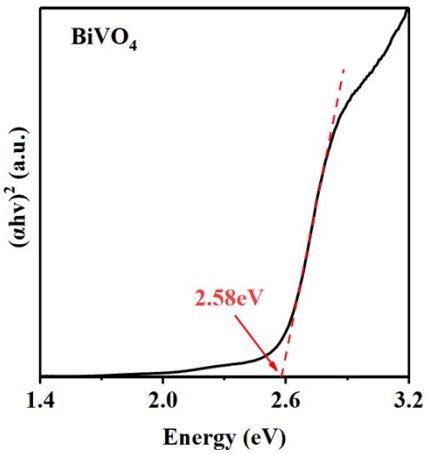

Figure S18. Tauc plots for $BiVO_4$ film.

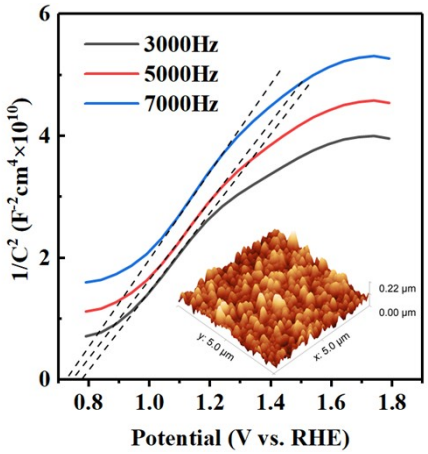

Figure S19. Mott–Schottky plots and AFM (insert) for $BiVO_4$.

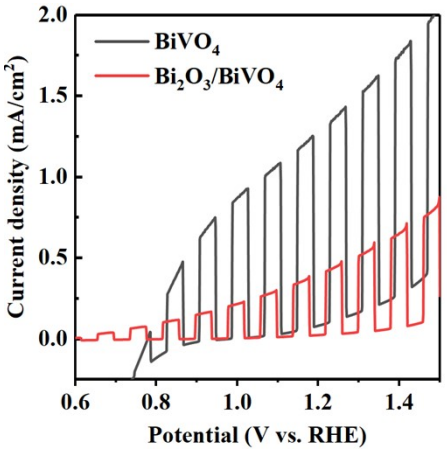

Figure S20. Chopped LSV scans for $BiVO_4$ and $Bi2O_3/BiVO_4$ photoelectrodes. The measurements were performed under AM 1.5 illumination.